Journal of the European Ceramic Society 20 (2000) 901–911

Application of probabilistic fracture mechanics to a dynamic loading situation using the example of a dynamic tension test for ceramics

Robert Danzer [a,*], Franz Dieter Fischer [b], Wen-Yi Yan [c,†]

[a] *Institut für Struktur und Funktionskeramik, Montanuniversität Leoben, Franz-Josef-Straße 18, A-8700 Leoben, Austria*
[b] *Institut für Mechanik, Montanuniversität Leoben, Franz-Josef-Straße 18, A-8700 Leoben, Austria*
[c] *Christian Doppler Laboratorium für Funktionsorientiertes Werkstoff-Design, Montanuniversität Leoben, Franz-Josef-Straße 18, A-8700 Leoben, Austria*

Received 4 February 1999; received in revised form 19 July 1999; accepted 8 August 1999

Abstract

Every acceleration or deceleration causes inertia forces and as a consequence elastic waves. Of course, such dynamic loading situations often occur in structural applications of materials. The consequences of such dynamic loading on designing with ceramics are considered on the example of a new dynamic tension test. First, the test device is described, and the resulting loading situation is carefully analysed. It is seen that the dispersive character of wave propagation causes an inhomogeneous stress distribution changing with time. Then the influence of the dynamic loading on the stress intensity factors of small cracks, which in general are responsible for failure in ceramic materials, is discussed. Finally, the consequences on fracture statistics are considered. Although the demonstrated procedure is restricted to not-too-steep ramps of the wave front, it is considered to be valid for most cases of dynamically loaded ceramic components. Exceptions are very sharp impact or ballistic loading.

Keywords: Dynamic loading; Fracture statistics; Mechanical properties; Mechanical testing

1. Introduction

In brittle materials, e.g. ceramics, failure under tensile loading generally starts at flaws which are distributed within the specimen or at its surface. The size and orientation of the fracture initiating flaws is decisive for the strength of the specimen. The strength varies from specimen to specimen since the size and orientation of these flaws varies from specimen to specimen. This causes the large scatter of strength data of brittle materials. An important, technical consequence of this behaviour is the dependence of the strength on the size of the specimen.[1,2] More than 50 years ago, Weibull[3,4] defined an empirical fracture statistics, which properly describes these features of the fracture behaviour of brittle materials. Up to now it provides the scientific basis of the generally accepted design procedure with ceramics.[5]

Although quasi-static load spectra predominate in most applications of ceramic components, the inertia force cannot be neglected in some applications. Examples are quickly operating valves or — as reported recently[6,7]— electrical resistors loaded by very short electrical pulses, e.g. caused by lightening (due to Joule heating they want to expand, and this is opposed by the inertia force). Current fracture statistics are formulated for quasi-static loading conditions. In this paper, the extension of fracture statistics to dynamic loading situations is demonstrated on the example of a recently proposed dynamic tension test.[8]

The test set-up is described in the following section. The dynamic stress field is analysed in Sections 3 and 4. Section 5 deals with the calculation of dynamic stress intensity factors. The fracture statistical principles are summarised in Section 6 and then applied to the dynamically loaded rod in Section 7.

* Corresponding author.
† Present address: Department of Mechanical Engineering, Imperial College, London, UK.

0955-2219/00/$ - see front matter
PII: S0955-2219(99)00219-8

2. Description of a dynamic tension test device

A rod-like specimen travelling with a well-defined constant velocity, v, is suddenly stopped at its trailing end. Due to the inertial force a tensile stress wave propagates along the rod. The maximum tensile stress amplitude of the wave is directly related to the velocity of the rod before it is stopped and can be estimated by the impact of a rod using a simple one-dimensional analysis, see e.g. Achenbach[9] (p. 344), as

$$\sigma = E\frac{v}{c_o} \text{ for } 0 \leqslant x \leqslant c_o t \leqslant L, \tag{1}$$

E is the Young's modulus, c_o is the speed of sound in the material under investigation with density ρ and is given by $c_o = \sqrt{\frac{E}{\rho}}$ for the one-dimensional case, L is the length of the specimens, x is the spatial coordinate and t is the time. Of course, the tension wave is reflected at the free end ($x = L$) as a compressive wave which leads to a partial extinguishing of the stress.

Thus the strength of the specimen can be measured by repeated testing with gradually increasing velocities, until the specimen breaks. Another possible application of this testing principle is the proof testing of rods or rod-like components. Dynamic tensile testing can also be carried out in an alternative way, by suddenly accelerating the specimen from its front end to a specified velocity v.

In general, both types of testing principles seem to work much more simply and more directly than Hopkinson pressure bar devices for ceramic bar testing.[10] The principle and examples of technical realisation are described more precisely in a recent patent of Fischer and Danzer.[11] In his diploma thesis, Stickler[5] demonstrated a practical realisation of the new dynamic tensile testing principle by applying the alternative way of accelerating a specimen which is initially at rest. Slender rod-like specimens made of brittle recrystallized molybdenum were thermally shrunk into a cylindrical carrier on their front end. By impinging the specimen-carrier from its back end the whole assembly can be suddenly accelerated. This induces a tensile stress wave that propagates in the opposite direction axially through the specimen. A number of specimens were broken by repeated testing with a systematic increase of the impact velocities and, consequently, the stress wave magnitudes. The strength of the specimens was evaluated according to Eq. (1).

In the following the accuracy and practical applicability of the proposed method of testing is assessed. Four effects are studied in detail:

- The exchange of energy with a deformable seat, which may lead to an increase of the longitudinal stress above the value of Eq. (1).
- The dispersive character of the wave propagation due to radial inertial effects and, therefore, the actual finite geometry of the specimens. As will be seen, locally significant stress concentrations may occur.
- The influence of the wave propagation on the stress intensity factors of pre-existing cracks leading to dynamic stress intensity factors.
- The application of fracture statistics on dynamic loading situations.

3. Energy exchange between the specimen and the seat

The specimen can be modelled in the simplest case by a cylindrical rod of length L as in Fig. 1. In this section the rod is assumed to be very slim and only the one-dimensional case is analysed. The displacement of the rod is u, $\frac{\partial_u}{\partial_t}$ its velocity. Since we investigate the practically realised device, see Stickler,[8] we assume the right end of the rod to be connected to a seat S. At time $t = 0$ the seat is suddenly subjected to a velocity v.

Since, at this point, we are mainly interested in the modification of the maximum stress due to the deformablity of the seat, it is modelled for the sake of simplicity by a linear spring with the spring constant k. The force in the spring at time t is

$$k(u + vt) = EA\frac{\partial_u}{\partial_x}, \tag{2}$$

since it must be equal to the force in the bar with the cross-section area A.

The initial/boundary value problem can be written as

$$0 \leqslant x \leqslant L, \quad c_o^2\frac{\partial^2 u}{\partial x^2} = \frac{\partial^2 u}{\partial t^2}, \tag{3}$$

$$x = 0, \quad u = -vt + \kappa\frac{\partial u}{\partial x}, \kappa = \frac{EA}{k}, \tag{4}$$

$$x = L, \quad \frac{\partial u}{\partial x} = 0. \tag{5}$$

Since the bar is initially at rest, it follows that at

$$t = 0, \quad u = 0, \frac{\partial u}{\partial t} = 0. \tag{6}$$

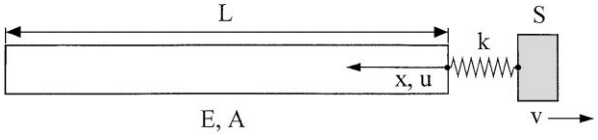

Fig. 1. Cylindrical specimen as rod model.

The problem can immediately be substituted by a homogenous boundary value problem by introducing

$$u = -vt + \tilde{u}. \tag{7}$$

$\tilde{u}$ is the solution of the homogenous boundary value problem defined now as

$$c_o^2 \frac{\partial^2 \tilde{u}}{\partial x^2} = \frac{\partial^2 \tilde{u}}{\partial t^2}, \tag{8}$$

$$x = 0, \quad \tilde{u} = \kappa \frac{\partial \tilde{u}}{\partial x}, \tag{9}$$

$$x = L, \quad \frac{\partial \tilde{u}}{\partial x} = 0, \tag{10}$$

$$t = 0, \quad \tilde{u} = 0, \frac{\partial \tilde{u}}{\partial t} = v. \tag{11}$$

Of course, for $\kappa = 0$ the maximum stress is Ev/c_o [see Eq. (1)]

A Laplace transformation technique can be used to find a solution for $\kappa \neq 0$. Details of the solution can be taken from the paper by Werner and Fischer.[12] The boundary condition Eq. (9) introduces a dispersive character to the solution. During the second and subsequent reflections of the wave the stress state may even be increased in relation to $\sigma = Ev/c_o$. For the sake of demonstration, a dimensionless stress $\tilde{\sigma} = \sigma c_o/(Ev)$ and a dimensionless time $\tilde{t} = tc_o/L$ are introduced. Fig. 2 shows the stress at $x = L/2$ over the time depending on $\tilde{\kappa}$ ($\tilde{\kappa} = 0.025$ and 0.1). Fig. 3 demonstrates the time envelope over the maximum stress in the rod in dependence on $\tilde{\kappa}$. It is interesting to note that a deformable seat may lead to an increased maximum stress in the rod after several reflections. This effect, however, can be ignored during the propagation of the first tension wave, especially if the seat slows down and the specimen separates from the seat.

4. Dispersion and stress concentrations

Obviously the one-dimensional problem formulation ignores the radial inertial effect, which leads to a dispersive character of the solution, also for $\kappa = 0$. Rayleigh and later Love (Ref. 13, p. 248) were aware of this effect and added a correction term $-\nu^2 \frac{R^2}{2} \frac{\partial^4 u}{\partial x^2 \partial t^2}$ to the wave propagation described in Eq. (1); R is the radius of the rod and ν is Poisson's ratio. Davies[14] proved both experimentally and analytically this dispersive character. Recently Fiedler and Wenzel[15] reported an error in Davies analytical solution.

Taking into account the dispersive character of the wave propagation one can start with the treatment of a circular cylinder considering the uniform wave propagation in a half-space [see, e.g. Achenbach[9] (p. 21 ff) or Bedford and Drumheller[16] (p. 47)]. The wave propagation speed

$$c_1 = \left(\frac{1-\nu}{(1+\nu)(1-2\nu)}\right)^{1/2} c_o \tag{12}$$

is that of a dilatational wave. The half-space solution consists of only one nonzero displacement component, namely $\tilde{u}_h$ in x-direction. The immediate consequences are:

- The stress component $\sigma_{x,h}$ follows as

$$\sigma_{x,h} = \left(\frac{1-\nu}{(1+\nu)(1-2\nu)}\right)^{1/2} E\frac{\nu}{c_0}, \; 0 \leqslant x \leqslant c_1 t, \tag{13}$$

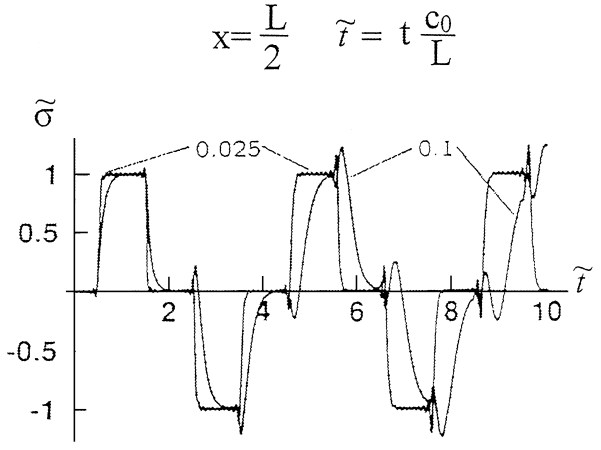

Fig. 2. Relative longitudinal stress $\tilde{\sigma}$ history in a moving rod, suddenly elastically fixed at its trailing end; dimensionless spring constant $\tilde{\kappa}$.

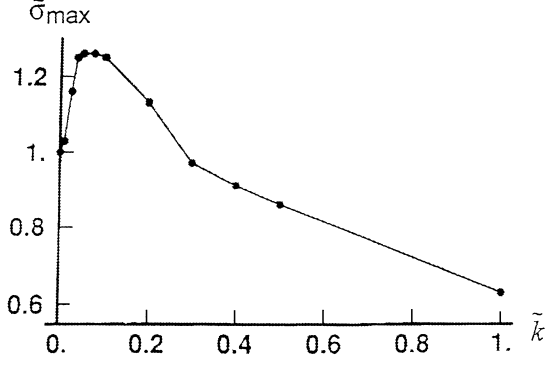

Fig. 3. Maximum relative longitudinal stress $\tilde{\sigma}_{\varepsilon,max}$ in a moving rod, suddenly elastically fixed at its trailing end in dependence of the dimensionless spring constant $\tilde{\kappa}$.

which results in a 16% higher longitudinal stress for $\nu = 0.3$ compared with the one-dimensional rod solution.

- Two further stress components $\sigma_{y,h}$, $\sigma_{z,h}$ in the transverse direction appear as

$$\sigma_{y,h} = \sigma_{z,h} = \frac{\nu}{1+\nu}\sigma_{x,h}, \quad 0 \leqslant x \leqslant c_1 t, \tag{14}$$

$$\sigma_{y,h} = \sigma_{z,h} = 0, \quad x > c_1 t.$$

- To achieve, therefore, the solution for a circular cylinder as a cylindrical "cut-out" of a half-space, the corresponding solution must be superposed on a further solution, according to a negative radial stress $\sigma_r = -\sigma_{y,h} = -\sigma_{z,h} = -\frac{\nu}{1+\nu}\sigma_{x,h}$ for $x < c_1 t$ and 0 for $x \geqslant c_1 t$ to assure a stress-free surface of the cylinder.

  The axisymmetric problem formulation has consequently to deal with two wave propagation phenomena:
- a dilatational wave propagating from the fixed end of the cylinder ($x = 0$) in the longitudinal direction, represented by the homogenous half-space solution;
- dilatational and shear waves propagating from the cylindrical surface into the cylinder in radial and longitudinal directions.

This additional wave field is named "von Schmidt wave" [see, e.g. the book by Lin[17] (chapter 3.3.5) or the paper by Valeš et al.[18]]. The corresponding displacement and stress field make it necessary to solve a rather complex boundary/initial value problem. The von Schmidt wave gives rise to the dispersive character of the stress field. To the knowledge of the authors the first person to tackle this problem was Skalak,[19] applying integral transforms. However, only an approximate method for the evaluation of the inverse transforms, in this case the "saddle point method", was used. Therefore, Skalak's relations for displacements and stresses are valid only for a certain time after the impact and a certain distance ahead of the place of impact. The "head" of the longitudinal stress wave is not a "jump" as in the case of a rod but a "steep ramp". Due to the dispersive character an increase of the stress level of 25 to 30% in relation to the one-dimensional solution can be found. This represents a rather high "overstress" in relation to the one-dimensional solution. The full picture of the deformation and stress state was very recently presented by Valeš et al.,[18] without any approximations in the inversion of the integral transforms. They showed, specifically, in the region $0 \leqslant x \leqslant 3R$, that a very inhomogenous stress field appears. The stress σ_x may even show a peak ("a spike") somewhere between $0 \leqslant r/R \leqslant 1$. Locally the stress may rise more than 35% in relation to the one-dimensional solution. Finally it should be mentioned that Valeš et al.[18] evaluated the displacement field as an infinite series of improper integrals. Significant numerical efforts are necessary to obtain a satisfying picture of the solution. Especially it is difficult to perform accuracy checks for the numerical evaluation of their integrals. At least an overall qualitative check of the results by following the energy content of the specimen would be of high value.

A concept overcoming the difficult operations with respect to the inversion of the integral transforms can be an a priori numerical concept (in the literature very often the finite difference method has been used[20] and later along the bicharacteristics of the governing differential equations[21]). The authors of this paper prefer to use the finite element method, specifically with respect to its broad applicability and its accuracy checks. In the following, ABAQUS-Explicit[22] is used.

A dimensionless problem formulation is introduced by the following entities:

$x = \xi R$, ξ... dimensionless length co-ordinate,

$r = \eta R$, η... dimensionless radial co-ordinate,

$u_\xi = \tilde{u}_\xi\left(\frac{v}{c_o}\cdot R\right)$ $\tilde{u}_\xi$... dimensionless longitudinal displacement,

$u_\eta = \tilde{u}_\eta\left(\frac{v}{c_o}\cdot R\right)$ $\tilde{u}_\eta$... dimensionless radial displacement,

$t = \tilde{t}\left(\frac{R}{c_o}\right)$ $\tilde{t}$... dimensionless time.

Two types of boundary conditions at $\xi = 0$ are studied:

$\tilde{u}_\xi = 0$, $\tilde{u}_\eta$ free: "fixed end",

$\tilde{u}_\xi = 0$, $\tilde{u}_\eta = 0$: "clamped end".

It can easily be shown that the Navier equations of elasticity, expressed in the dimensionless displacements $\tilde{u}_\xi$ and $\tilde{u}_\eta$ contain only two factors, namely $(1-2\nu)$ and $2(1+\nu)$. The corresponding numerical problem formulation can be represented by a substitute specimen of a radius"1", the Young's modulus "1" and the density "1". Only the dimensionless length L/R is a variable entity. As a parameter Poisson's ratio is fixed first as $\nu = 0.29$ (the value of siliciom nitride ceramics). The actual stress components can be found by multiplying the calculated stresses by the factor Ev/c_o. Therefore, the resulting longitudinal stress $\tilde{\sigma}_\xi$ reflects directly the relative variation of the actual stress field in relation to the one-dimensional stress with the dimensionless value "1".

A specimen with ratio $L/R = 40$ is investigated. Twenty square-shaped, constant strain elements are used over the radius, so $800 \times 20 = 16{,}000$ elements exist. At each time step the energy content of the system, which must remain constant, is checked. Deviations much smaller than 10^{-4} of the (constant) energy content can be observed.

We consider the time interval [0, L/R], which means we inspect all instants until the one-dimensional wave would have reached the right end of the rod at $x = L$. During this time interval the maximum longitudinal stress $\sigma_{\xi,\max}$ as well as the maximum principle stress in each volume element are stored. Next charts were drawn giving a "time envelope" over the maxima of the stress state within [0, L/R]. In the following context, the "fixed end" boundary condition is taken into account. Fig. 4 demonstrates isolines for $\tilde{\sigma}_{\xi,\max}$ over the whole specimen. Three regions can be distinguished within $0 \leqslant \xi \leqslant 40$:

1. The "(trailing) end" region covering the area $0 \leqslant \xi \leqslant$ ca. 7, where a very inhomogeneous stress state can be observed with a stress level higher than 1.46. Details can be taken from Fig. 5, which represents a magnification of the "(trailing) end" region with a finer grading of the isolines. Surprisingly high values of $\tilde{\sigma}_{\xi,\max}$ near the axis can be detected. The maximum value of $\tilde{\sigma}_{\xi,\max}$ amounts to 2.42. Since the paper of Valeš et al.[18] concentrates more on $\tilde{\sigma}_{\xi,}$ near the surface, such a high value of $\tilde{\sigma}_{\xi,\max}$ is not reported. However, near the surface, the values $\tilde{\sigma}_{\xi,\max}$ agree well with the results of Valeš et al.[18] for a semi-infinite cylinder.
2. The "middle" region covering the area $[7 \leqslant \xi \leqslant 36]$, from which a more detailed view can be taken from Fig. 6. Most of the $\sigma_{\xi,\max}$values lie the range between the "B"-isoline and the "D"-isoline representing values between 1.24 and 1.34. This range corresponds to the value of the "head" of the stress wave found by Skalak.[19]
3. The "head" region covering the area $36 \leqslant \xi \leqslant 40$ shows clearly the "steep ramp" character of the head of the stress wave decreasing from 1.24 to 0.

If the "clamped end" boundary condition is dealt with, only the "(trailing) end" region and, therefore, the area between $(0 \leqslant \xi \leqslant 1)$ near the free surface at $\eta = 1$, is concerned. Here a local increase of $\tilde{\sigma}_{\xi,\max}$ to values higher than 1.70 can be observed.

Finally it can be concluded that at least over ca. 11/40 of the whole specimen length a very inhomogeneous stress state occurs. Locally the increase in relation to the rod solution amounts to more than a factor of 2. The dispersive character of the wave propagation process can, therefore, not be ignored. The time history of the total kinetic energy and the total strain energy, however,

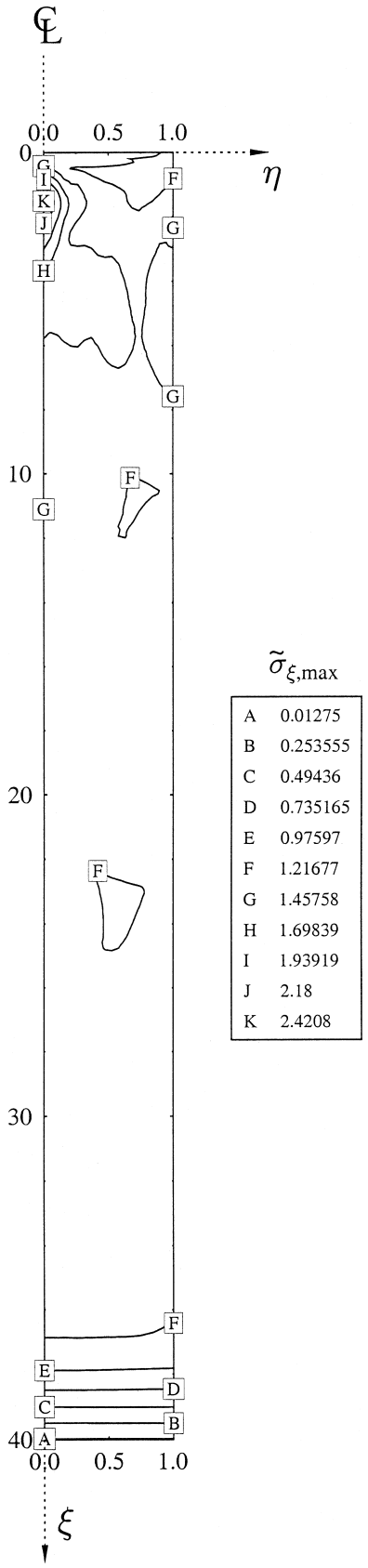

Fig. 4. Isolines for the maximum relative longitudinal stress $\tilde{\sigma}_{\xi,\max}$ in the whole specimen during the dimensionless time period [0,L/R], $\nu = 0.29$.

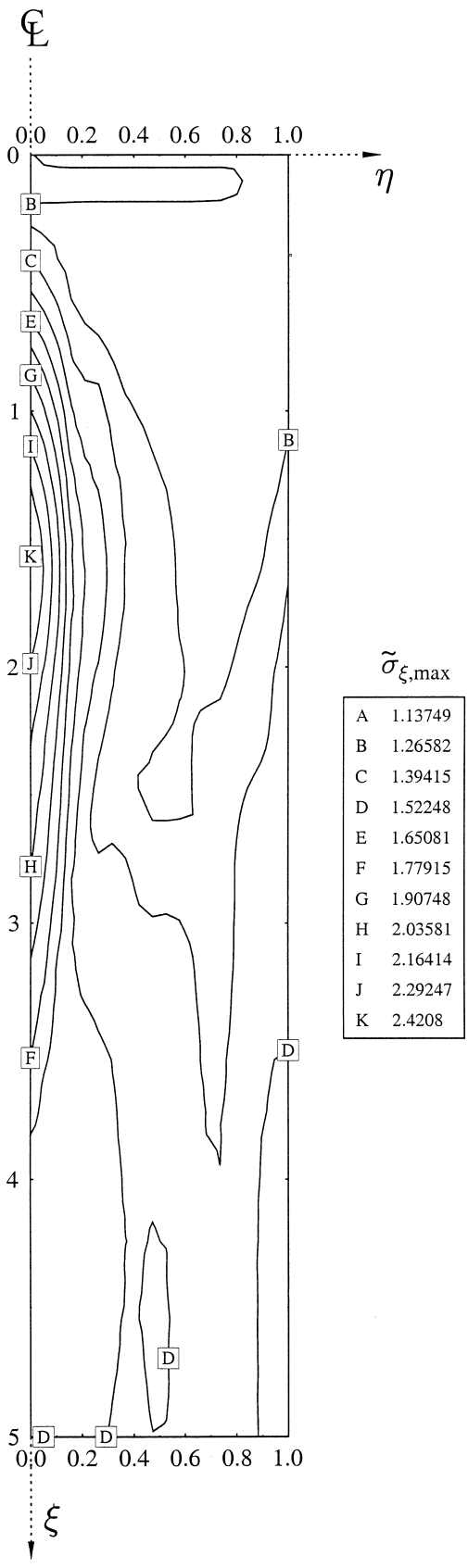

Fig. 5. Isolines for the maximum relative longitudinal stress $\tilde{\sigma}_{\xi,\max}$ in the "end" region during the dimensionless time period $[0,L/R]$, $\nu = 0.29$.

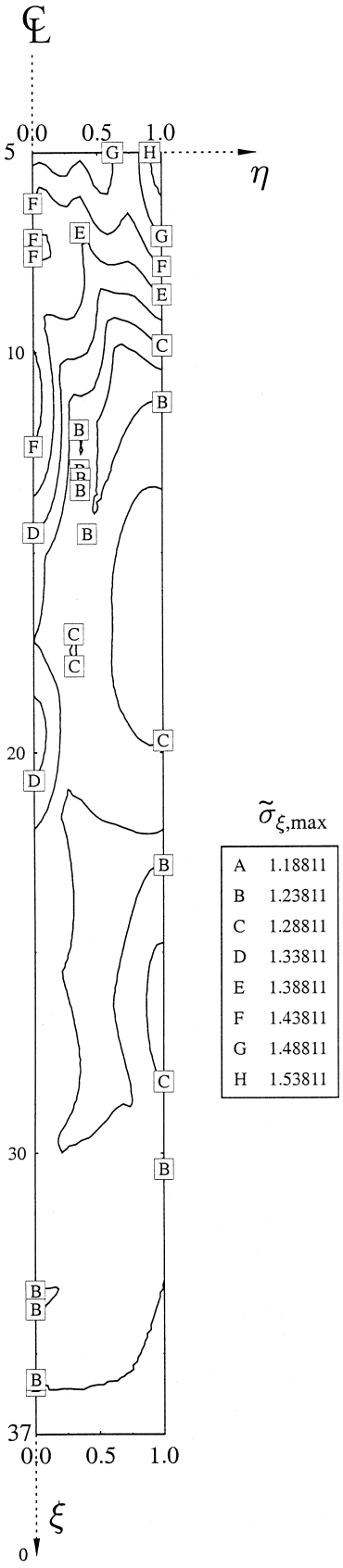

Fig. 6. lsolines for the maximum relative longitudinal stress $\tilde{\sigma}_{\xi,\max}$ in the "middle" region during the dimensionless time period $[0,L/R]$, $\nu = 0.29$.

coincides exactly with those for the uniaxial rod. The total strain energy increases linearly within the time interval $0 \leqslant \tilde{t} \leqslant L/R$ to its maximum value which corresponds to the initial overall kinetic energy. Thus the dispersive character of wave propagation cannot be detected in the energy balance. This fact, however, may be considered as a trivial check.

5. Dynamic stress intensity factor

If a stress wave front hits the surface of a small crack it is partially reflected as well as modified to a Rayleigh wave (in the following, for simplicity, only small penny shaped cracks of radius a are analysed). This gives rise to an increase of the stress intensity factor K_I, above its static value $K_{I,st} = \frac{2}{\pi}\sigma\sqrt{a\pi}$, where σ is the local stress amplitude in the uncracked body. The ratio $K_I/K_{I,st}$ depends on the steepness of the ramp of the wave front. Zhang and Gross[23] carefully investigated this dynamic crack problem. They introduced the dimensionless parameter $c_2\tau/a$, where c_2 is the shear wave velocity, which is in the order of magnitude of c_o, and τ is the "ramp" time interval during which the stress would increase linearly from 0 to its maximum value. The value of c_2 is $c_2 = 0.62c_o$ for $\nu = 0.29$. In Fig. 7, $K_I/K_{I,stat}$ is plotted as a function of $c_2\tau/a$ using the data of Zhang and Gross.[23] The ratio achieves a maximum of 1.3 for $\tau = 0$ and approaches zero $c_2\tau/a \rightarrow \infty$. It is less than 1.05 for $c_2\tau/a \geqslant 4$.

Due to the dispersive character discussed, a stress ramp really does exist. The "ramp" time interval τ can be taken from Skalak's solution,[19] by substituting the time, when the stress ramp starts, by x/c_o as

$$\tau = 4\left(\frac{\nu^2 R^2}{4c_o^2}\cdot\frac{x}{c_o}\right)^{1/3}. \tag{15}$$

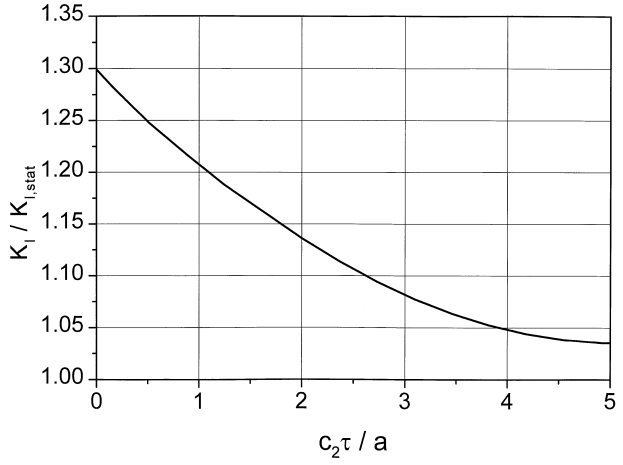

Fig. 7. Ratio of the stress intensity factor to its quasistatic limit versus the dimensionless parameter $c_2\tau/a$.

The dimensionless paramater $c_2\tau/a$ follows now as (again we set $\nu = 0.29$):

$$c_2\tau/a = 4(0.62)\left(\nu^2/4\right)^{1/3}\cdot\left(R^2x/a^3\right) \approx 0.7R^{2/3}x^{1/3}x/a. \tag{16}$$

It can be seen that $c_2\tau/a$ finally depends on the geometry (it is proportional to $R^{2/3}$), on the position x along the rod (it is proportional to $x^{1/3}$) and on the radius of the size of the investigated defect (it is inversely proportional to a).

For $c_2\tau/a \gg 1$ the dynamic stress intensity factor is approximately equal to the static value. In consequence of Eq. (16), this is not possible in an area around the fixed end of the rod (for very small values of x). In the following the typical situation of a tensile test performed on a specimen made of an advanced ceramic material is analysed: the size of the zone where the stress intensity factor is strongly influenced by dynamic effects, i.e. arbitrarily defined $K_I/K_{I,stat} \geqslant 1.05$, is given by $c_2\tau/a \leqslant 4$ (see Fig. 7). The length x can be calculated using Eq. (16). In advanced ceramics, the fracture initiating crack has in general an equivalent radius of 100 μm or less. A typical radius of a tensile test bar is around 3 mm. Using these assumptions the length of the influenced zone is around 20 μm, which is about 1/5 of the radius of the fracture initiating defect. For smaller fracture initiating defects, the zone size is even smaller. This finally means that this zone can be neglected and that the stress intensity factors in this dynamic study can be calculated from the "standard" relations for static stress intensity factors.

6. Basic principles of fracture statistics

A brief summary of the fracture statistics of brittle fracture is given. Then the consequences with respect to an inhomogeneous and transient stress field as would appear in the testing device are considered.

It is assumed that brittle fracture originates at flaws of different sizes statistically distributed within the specimen and on its surface. Therefore, the strength of a brittle material is also a statistic variable. Any flaw will be critical, if it is large enough to initiate fracture under a given stress field. Provided the density of flaws is so low that they do not interact and that any critical flaw will cause the specimen to fail (weakest link hypothesis), the probability of failure P_f is given by

$$P_f = 1 - \exp(-N_c), \tag{17}$$

where N_c is the mean number of critical flaws taken over a large set of specimens.[24] The mean number of critical flaws depends on the load amplitude (more flaws

become critical as the load increases) as well as on the specimen size. Assuming that the size of a flaw can be characterised for simplicity by a single parameter a (e.g. the radius of a penny-shaped crack) and that the Griffith fracture criterion holds, any crack is critical if its size is equal or larger than

$$a_c = \left(\frac{1}{Y}\frac{K_{Ic}}{\sigma}\right), \tag{18}$$

where σ is the applied tensile stress in the uncracked body normal to the plane of the flaw, Y is a geometry factor and K_{Ic} the fracture toughness of the material. For a spatially constant stress and a uniform distribution of flaws, the mean number of critical flaws equals the local density of critical flaws multiplied by the volume. For a non-uniform stress field and/or non-uniformly distributed flaws the mean number of critical flaws is obtained by integrating the local density of critical flaws over the volume as

$$N_c = \int_V \left(\int_{a_c}^{\infty} g(a, \underline{r})\mathrm{d}a\right)\mathrm{d}V, \tag{19}$$

where $g(a, \underline{r})$ is the frequency distribution density per unit volume of flaw sizes, a, at a point defined by the position vector $\underline{r}$. Even for a uniform distribution of flaws in the case of a non-homogeneous loading, the local density of critical flaws, given by the inner integral in Eq. (19), varies over the volume since, according to Eq. (18), the lower limit of integration depends on the stress at the position $\underline{r}$.

If the frequency distribution density in a homogeneous material is a monotonically decreasing function of the flaw size, $g(a)$, it can be approximated (at least in a small size region near to a_c) by an inverse power law $g(a) = g_o a^{-r}$, r being a material constant.[25,26] Then Eq. (17) can be transformed into the well known Weibull distribution (see, e.g. Freudenthal[25] and Danzer[24]) as:

$$P_f = 1 - \exp\left(-\frac{1}{V_o}\int_V \left(\frac{\langle\sigma\rangle}{\sigma_0}\right)^m \mathrm{d}V\right). \tag{20}$$

The Weibull parameter m is directly related to r by $m = 2(r-1)$. Therefore, it reflects the distribution of critical flaw sizes. σ_0 is the characteristic strength of a sample of specimens of size V_0. The notation $\langle\sigma\rangle = \begin{cases} \sigma & \text{for } \sigma \geqslant 0 \\ 0 & \text{for } \sigma < 0 \end{cases}$ is used to indicate explicitly, that the volume integration must be performed only over the region loaded in tension.

In practice, the Weibull parameters m and σ_0 are directly determined as material constants by a statistical evaluation of measured values of strength (see, e.g. Wachtman[27] and Creyke et al.[2] In this way the distribution of lengths of the most severe flaws (including their random orientation) is indirectly measured, as well. A high value of the Weibull modulus m corresponds to small variations in strength, and thus in flaw sizes. Engineering ceramics distinguish themselves by Weibull moduli greater than 10.

The above considerations refer to a uniaxial state of stress. For multiaxial stress conditions an appropriately defined equivalent stress $\bar{\sigma}$ should be substituted for σ in Eq. (20). The proper definition of the equivalent stress for a multiaxial stress state is still subject to debate (see, e.g. Batdorf[28] and Thiemeier.[29] As a first approximation, the highest principal stress can be taken as an equivalent stress. This will also be assumed in the following context.

To consider the influence of the specimen size, it is usual to define an effective volume V_{eff} which stems from the relation:

$$N_c = (V_{eff}/V_0).(\sigma^*/\sigma_0)^m. \tag{21}$$

σ^* is a reference stress. The effective volume $V_{eff}(\sigma^*)$ is the volume of a hypothetical tensile specimen subjected to a homogeneous uniaxial stress state which has the same probability of failure as the specimen (component) under investigation at the reference stress σ^*. Alternatively, an effective stress σ_{eff} can be defined according to the formula,

$$(\sigma^*)^m V_{eff}(\sigma^*) = (\sigma_{eff})^m V_0, \tag{22}$$

for an inhomogeneous stress field. σ_{eff} represents the stress in a tensile specimen of the same volume as the real component which leads to the same probability of failure. Evidently, Eqs. (20) and (21) are based on the Weibull distribution function.

7. Application of fracture statistics to the evaluation of dynamic tension testing results

It has been shown recently,[30,31] that a large effective volume of the test specimens is required in order to check the assumptions on the distribution of flaw sizes made in Eqs. (19)–(21). In order to judge the benefits of the proposed dynamic tension test method in comparison to quasistatic tension tests[32] the effective volume of the new testing procedure has to be evaluated. Doing this fracture statistics has to be applied to a dynamic loading situation.

The effective volume can be calculated using Eqs. (19)–(22). Up to now, the proper definition of the stress σ for a dynamic loading situation is still not clear. For each volume element and in the considered time interval

the maximum occurring tensile stress amplitude has the biggest contribution to the probability of failure. Therefore it is proposed to insert for σ in Eq. (20) the time envelope over the maxima of the stress state $(\tilde{\sigma}_{\xi,\max})$.

The data are visualised in Fig. 8. The ratio of the effective volume to the volume of the rod, V_{eff}/V, is plotted against the Weibull modulus m for various values of the Poisson's ratio ν. The reference stress in this representation is taken to be the stress amplitude of the uniaxial solution given by Eq. (8), i.e. $\sigma^* = \sigma_0$. For the limiting case $\nu = 0$ the effective volume remains equal to the volume of the specimen regardless of the Weibull modulus, since in this case the envelope of the transient stress field equals the stress field in a quasi-static tensile specimen with spatially constant load stress. For realistic values of Poisson's ratio ν, however, the effective volume strongly depends on the Weibull modulus. The dependence of the effective stress on the Weibull modulus is shown in Fig. 9 for various Poisson's ratios.

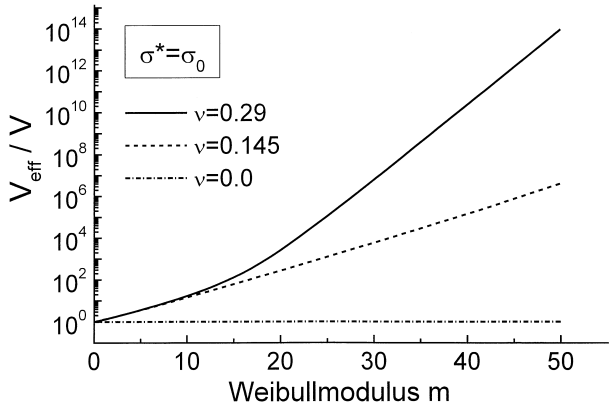

Fig. 8. Ratio of effective to real volume versus Weibull modulus for a reference stress $\sigma = \sigma_0$. The parameter used in the curves is the Poisson's ratio ν.

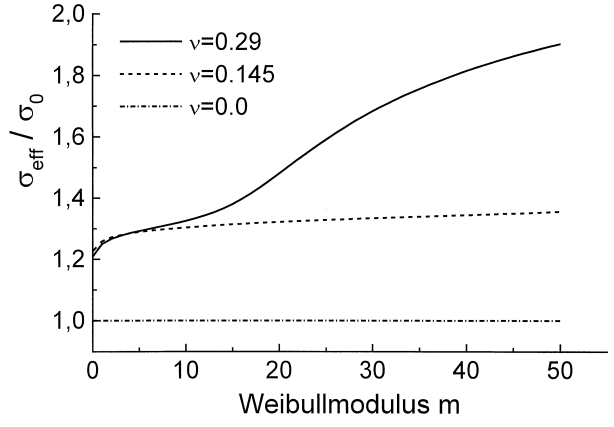

Fig. 9. Effective stress versus Weibull modulus, parameter in the curves is the Poisson's ratio ν.

As an example, we analyse the case of a modern structural ceramic, e.g. silicon nitride, which typically has $\nu = 0.29$ and $m = 20$. For the reference stress equal to the stress amplitude of the one-dimensional solution, $\sigma^* = \sigma_0$, the effective volume amounts to 3000 V_0 as can be seen from Fig. 8. According to Fig. 9, this fact leads to an effective stress about 1.5 times greater than in the case for $\nu = 0$. This considerable increase in the severity of loading due to the multiaxiality of the stress state means that, for the same probability of failure, the tensile specimen, quasi-statically loaded with the reference stress σ_0, should be 3000 times larger than the dynamically tested rod. Since the effective stress for $\nu = 0.29$ is 1.5 times higher compared to $\nu = 0$, the size of the failure initiating flaws amounts to, according to Eq. (8), about $1.5^{-2} = 0.44$ of that for $\nu = 0$ (which would correspond to the reference quasistatic tensile test). Such calculations are only valid provided that the conditions for the applicability of the Weibull theory are fulfilled and that the distribution of flaw sizes is of a Weibull type.

Fig. 10 shows a common representation of the dependence of the effective volume on the Weibull modulus. The reference stress is taken to be equal to the maximum principal stress component of the stress envelope and is different for each different value of Poisson's ratio ν. The numerical evaluations due to the Poisson's ratio ν of 0, 0.145 and 0.29, respectively, lead to the reference stress of 1, 1.59 and 2.35 times σ_0, respectively. This points to an increasing non-uniformity of the stress envelope with increasing Poisson's ratio ν. Therefore, the fraction of the specimen volume which sees the highest stress (taken as the reference stress) decreases. Additionally, the effect of the stress non-uniformity on the effective volume becomes stronger if flaw sizes become more uniform, characterised by higher m values. In the above numerical example the effective volume is as low as 10^{-3} V_o indicating the

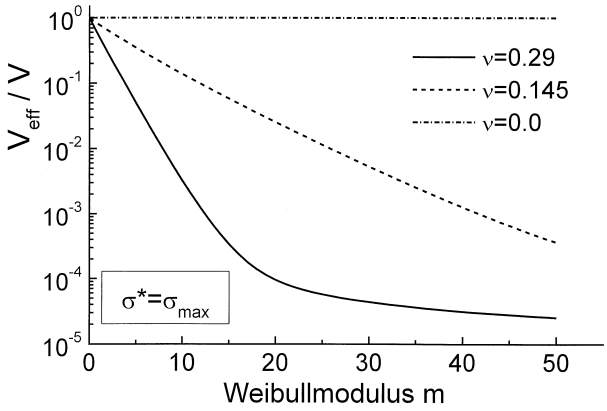

Fig. 10. Ratio of effective to real volume versus Weibull modulus. The reference stress is taken to be the maximum stress in each stress–time envelope; the parameter used in the curves is the Poisson's ratio ν.

relatively small size of the highest loaded region of the specimen. This is even less than the effective volume in a standard bending test.

8. Conclusion

For typical advanced ceramic materials (defined by a reasonably small size of the critical defect, e.g. a_c smaller than 100 μm) the dynamic and static stress intensity factors are equal unless in a very small zone. In a moving rod which is suddenly stopped at its back end, the extension of this zone is in the order of magnitude of the radius of the critical defect or even less.

Therefore a probabilistic analysis of the reliability can be performed for dynamically loaded bodies in analogy to the well known Weibull analysis for static situations. For the effective stress field in the Weibull distribution the time envelope of the highest principal tensile stress field has to be used (instead of the highest principal tensile stress field in the quasistatic case).

A one-dimensional analysis of a dynamic tensile test, which can be realised by sudden stopping of a moving bar at its trailing end, reveals a test situation with a spatially constant tensile stress state σ_0 throughout the specimen. However, in the real three-dimensional transient situation the transient stress field is strongly inhomogeneous.

The inhomogeneity of the transient stress field is caused by the dispersive behaviour of the elastic waves. In the analysed example the maximum principal tensile stress is 2.5 times higher than the tensile stress amplitude of the one-dimensional case.

Due to the brittle material behaviour and the inhomogeneity of the stress field the evaluation of the dynamic tension test necessitates a probabilistic analysis (e.g. Weibull). Such an analysis, which is standard for stationary situations, has been applied here to dynamic stress fields.

The analyses of the specimens show an extremely small effective volume, even smaller than the effective volume of a bending specimen of the same size. Since tests with a large relative effective volume are preferred in order to reduce the number of test specimens necessary to predict a high reliability, the transient character of stress fields makes this simple type of a tension test less attractive than expected.

The dynamic stress field and, as a consequence the effective volume of the dynamically loaded specimen, strongly depends on the Poisson's ratio ν, which points to the significance of radial dispersion of waves.

References

1. Davidge, R. W., *Mechanical Behaviour of Ceramics*. Cambridge University Press, London, 1979.
2. Creyke, W. E. C., Sainsbury, I. E. J. and Morell, R., *Design with Non-Ductile Materials*. Applied Science Publishers, London, 1982.
3. Weibull, W., *A Statistical Theory of the Strength of Materials*. Ingeniörsvetenskapsakademiens Handlingar No. 151, Stockholm, 1939.
4. Weibull, W., A statistical distribution function of wide applicability. *ASME Journal of Applied Mechanics*, 1951, **18**, 293–297.
5. Danzer, R., Ceramics: mechanical performance and life time prediction. In *Encyclopedia of Materials Science and Engineering*, Sup. Vol. 3 ed. R. W. Cahn and M. B. Bevers. Pergamon Press, Oxford, UK, 1993, pp. 1557– 1570.
6. Vojta, A. and Clarke, D. R., Electrical impulse induced fracture of zinc oxide varistor ceramics. *Journal of the American Ceramic Society*, 1997, **80**, 2086–2092.
7. Lengauer, M., Rubesa, D. and Darizer, R., Finite element modelling of the electrical impulse induced fracture of a high voltage varistor. *Journal of the European Ceramic Society*, in press.
8. Stickler, Ch., *Verfahren zur dynamischen Zugprüfung von keramischen Werkstoffen*. Diploma thesis, Montanuniversität Leoben, 1995.
9. Achenbach, J. D., *Wave Propagation in Elastic Solids*. North-Holland/American Elsevier Publishing Comp., Amsterdam, New York, 1975.
10. Najar, J. and Müller-Bechtel, M., Spalling fracture experiments with ceramic bars at elevated temperatures. *Archive of Mechanics*, 1997, **49**, 359–369.
11. Fischer, F. D. and Danzer, R., *Verfahren und Vorrichtung zur Prüfung der Zugfestigkeit eines spröden, stabförmigen Prüflings* (Procedure and device for testing of the tensile strength of brittle, rod-type specimens). Austrian patent 1657/96, 1996.
12. Werner, E. A. and Fischer, F. D., The stress state in a moving rod suddenly elastically fixed at its trailing end. *Acta Mechanica*, 1995, **111**, 171–179.
13. Love, A. E. H., *A Treatise on the Mathematical Theory of Elasticity*, 4th edn. Dover Publications, New York, 1944.
14. Davis, R. M., A critical study of the Hopkins pressure bar. *Philosophical Transactions of the Royal Society London*, 1948, **A240**, 375–457.
15. Fiedler, Ch. and Wenzel, W., Analytical approximate 3D solution for the longitudinal vibrating cylinder. *Archive of Applied Mechanics*, 1996, **66**, 447–459.
16. Bedford, A. and Drumheller, D. S., *Introduction to Elastic Wave Propagation*. John Wiley & Sons., Chichester, 1994.
17. Lin, X., *Numerical Computation of Stress Waves in Solids*. Akademie Verlag GmbH, Berlin, 1996.
18. Valeš, F., Morávka, St., Brepta, R. and Cerv, J., Wave propagation in a thick cylindrical bar due to longitudinal impact. *JSME International Journal Series A*, 1996, **39**, 60–70.
19. Skalak, R., Longitudinal impact of a semi-infinite circular elastic bar. *ASME Journal of Applied Mechanics*, 1957, **24**, 59–64.
20. Alterman, Z. and Karal, F. C. Jr., Propagation of elastic waves in a semi-infinite cyclindrical rod using finite difference methods. *Journal of Sound and Vibration*, 1970, **13**, 115–145.
21. Liu, K.-Sh., Li, X. and Tanimura, Sh., Two-dimensional stress wave propagation in a transversing isotropic cylinder. *JSME International Journal Series A*, 1997, **40**, 128–134.
22. Anon., *ABAQUS/Explicit User Manual*. Hibbit, Karlsson & Sorensen, Inc. Rhode Island, USA, 1997, Version 5.6.
23. Zhang, Ch. and Gross, D., Pulse shape effects on the dynamic stress intensity factor. *International Journal of Fracture*, 1992, **58**, 55–75.
24. Danzer, R., A general strength distribution function for brittle materials. *Journal of the European Ceramic Society*, 1992, **10**, 461–472.
25. Freudenthal, A. M., In *Statistical Approach to Brittle Fracture, Fracture: An Advanced Treatise, Vol. II: Mathematical Fundamentals*, ed. H. Liebowitz. Academic Press, New York, NY, 1968, pp. 591–619.

26. Jayatilaka, A. and Trustrum, K., Statistical approach to brittle fracture. *Journal of Materials Science*, 1977, **12**, 1426–1430.
27. Wachtman, J. B., *Mechanical Properties of Ceramics*. John Wiley & Sons, New York, NY, 1996.
28. Batdorf, S.B., In *Fracture: Statistical Theories, Encyclopedia of Materials Science and Engineering*. ed. M. B. Bever. Pergamon Press, Oxford, UK, 1986, pp. 1858–1864.
29. Thiemeier, T., *Lebensdauervorhersage für keramische Bauteile unter mehrachsiger Beanspruchung*. Doctor thesis, Fakultät für Maschinenbau der Universität KarIsruhe, 1989.
30. Danzer, R. and Lube, T., In *New Fracture Statistics for Brittle Materials. Fracture Mechanics of Ceramics*, Vol. 11, ed. Hasselmann et al. Plenum Publishing Corp., New York, 1996, pp. 425–439.
31. Danzer, R. and Lube, T., Fracture statistics of brittle materials: it does not always have to be Weibull statistics. In *Proc. of 6th Int. Symp. on Ceramics Materials and Components*, Japan Fine Ceramics Association, Tokyo, 1998, pp. 683–688 (ISBN 4-9980630-0-6).
32. Lube, T., *Entwicklung eines Zugversuches zur Zuverlässigkeitsanalyse von keramischen Ventilen*. Diploma thesis, Montanuniversität Leoben, 1993.